INTRODUCTION TO FTIR FOR USE IN DETECTION OF GAS PHASE ANALYTES

Charles M. Phillips

Environmental and Process Monitoring
Thermo Fisher Scientific
East Windsor, CT

INTRODUCTION

Fourier Transform Infrared Spectrometry (FTIR) has been a powerful technique used by many researchers and engineers for compositional analysis of all phases of matter, from solids to liquids and gases. However, to many, the FTIR is just a "black box" that produces data without understanding how those data are formulated. In this talk, we will investigate the theory behind FTIR to provide insight into the utilization and limitations of this spectroscopic technique. This talk will cover the basic theory of FTIR; how the spectral data are created from the raw optical signal; how these spectra are processed into quantifiable results and how these results are used to provide a useful analytical tool for gas phase compositions. We will focus on a couple applications used in research and engineering which are advancing the technology: carbon capture, utilization and storage (CCUS), and air separation unit (ASU) gas purity.

THEORY

The nature of light has always intrigued mankind. It is both considered as a cluster of quantized particles ("photons") or as a series of electromagnetic "waves". This particle/wave duality was investigated by several famous Nobel winning physicists, among which were: Max Planck, Albert Einstein and Albert Michelson. Their groundbreaking theories and experiments helped to reveal how light could have this duality and to use these properties in novel and useful ways. In particular, we will return to Michelson later on.

Infrared spectroscopy

All forms of matter are comprised of atoms which vibrate among their interatomic bonds. These vibrations commonly occur in the infrared portion of the electromagnetic spectrum (red region in Figure 1).

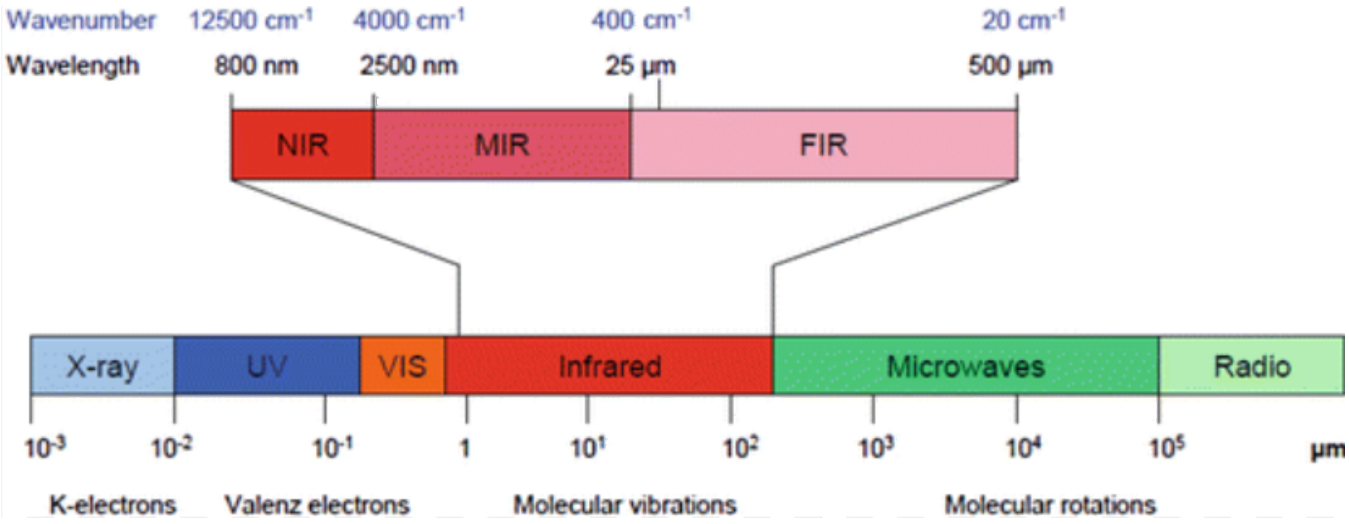


Figure 1. Electromagnetic spectrum from radio waves to X-rays

The wavelengths encompassing the infrared region run from 800 nm (near-IR) to 50000 nm (far-IR). Here is where radiation probes these various vibrations. However, not all atomic and molecular motion responds to this radiation. There are "selection rules" for these motions which must be met to induce an infrared spectrum. The primary consideration is that there must be a change in the dipole moment of the molecule during the vibration. This rules out what are known as "homonuclear diatomics" such as O_2, N_2, Cl_2, F_2 since the vibration along the molecular bond is totally symmetric around a central point (see Figure 2). In addition, monatomic species (Xe, Kr, Ar) do not have an infrared spectrum since they possess no molecular bond. Certain selected members of these types of gases are used as a reference zero in an FTIR (to be explained later on).

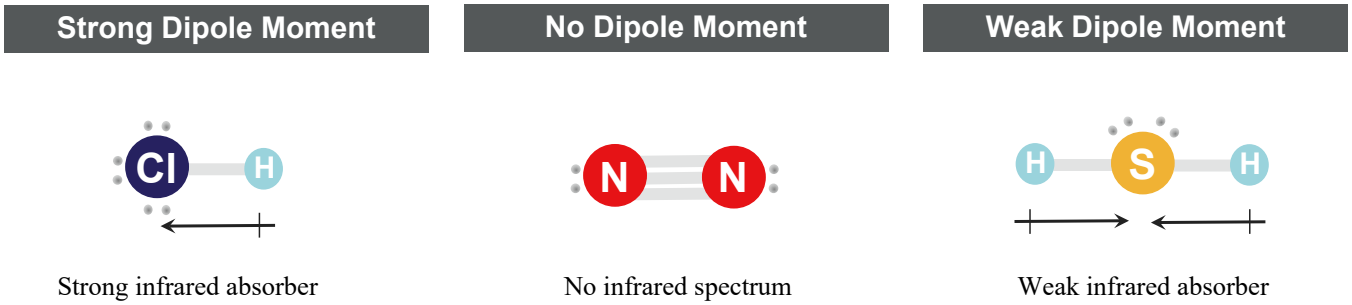


Figure 2. Three cases of molecular dipole moments

Since this topic will be discussion of FTIR to gas phase samples, there is a definite distinction between this and condensed phase infrared spectra. Namely, the fact that in gas phase, molecules do not only vibrate, but they can also rotate as well, schematically (Figure 3):

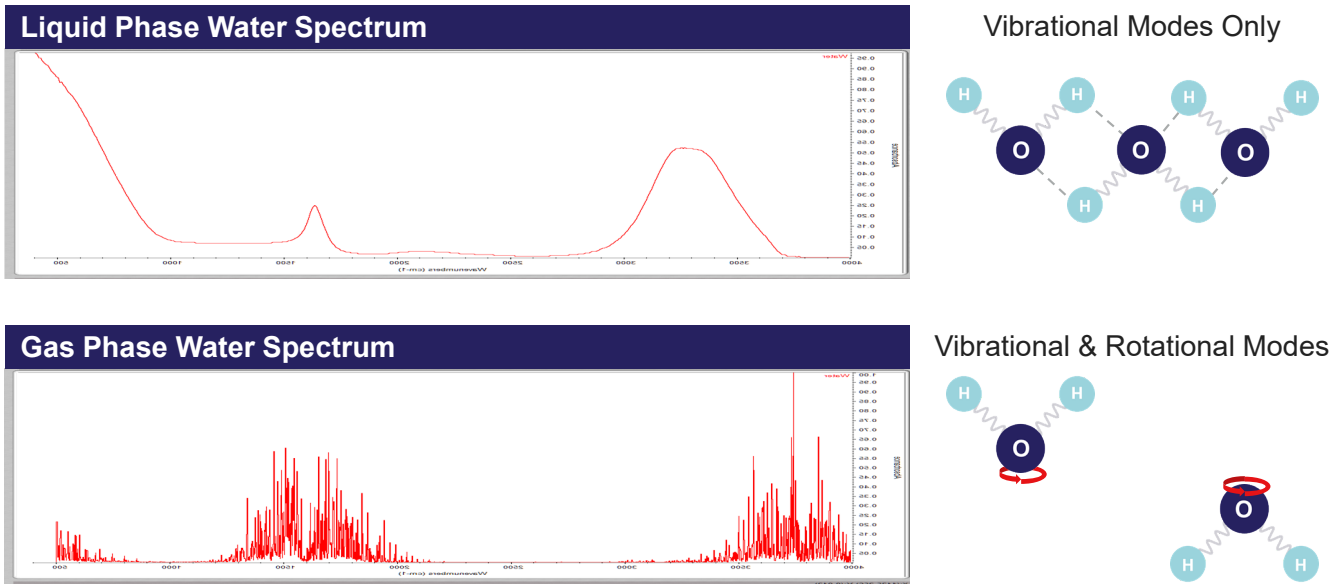


Figure 3. Comparison of liquid and vapor phase water spectra

The fine structure in the gas phase water spectrum is due to the fact that not only are vibrations "quantized" (i.e., have distinct energy levels which are determined by quantum mechanics), but rotations are also quantized. As the molecules get heavier (higher molecular weight), the gap in the rotational energies is so small that they "smear out" and look more like a condensed phase spectrum, even though they are rotating.

Before the advent of FTIR, most researchers used a dispersive prism or grating based infrared spectrometer (Figure 4), but the principle behind acquiring an infrared spectrum is the same. A heated source (usually a glowbar ceramic heated to 1000º C) emits infrared radiation which is incident on an entrance slit and then collimated by a lens or parabolic reflector. This light is transmitted onto the prism or grating and broken up into the various infrared frequencies by their dispersive properties.

Each frequency passes through an exit slit and onto the sample, where the transmitted light is measured by an appropriate infrared detector. Unfortunately, since so much of the light is "thrown away" at any one time, these spectrometers were notoriously insensitive. We will discuss how FTIR has greatly improved sensitivity by orders of magnitude, but to do this we will have to explore the basis of interferometry and the Fourier Transform.

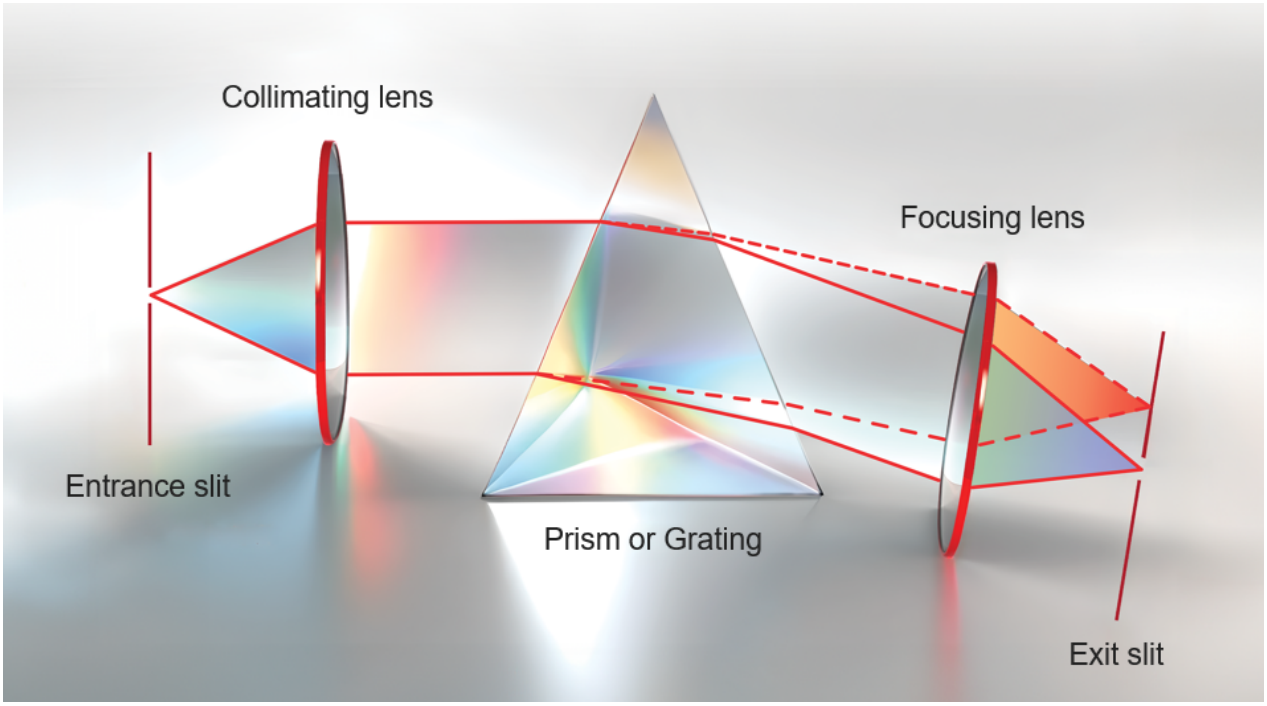


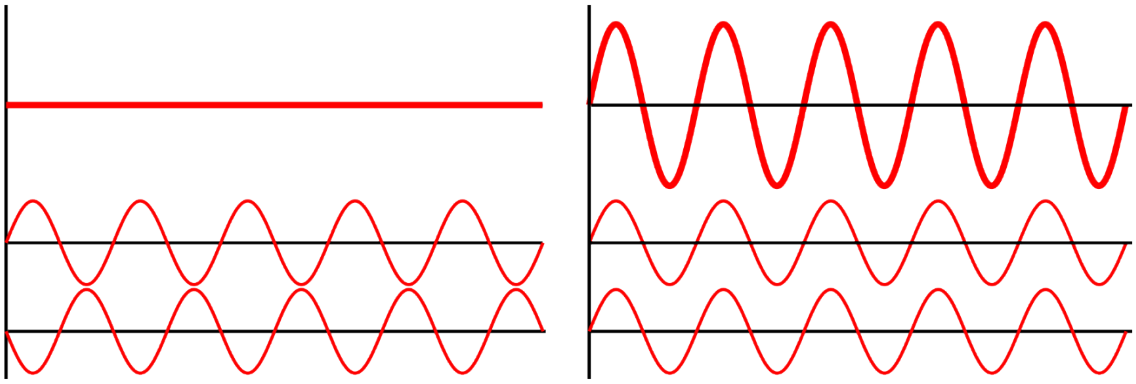
Figure 4. Dispersive Infrared Spectrometer

Interferometry and Fourier Transforms

As initially mentioned in the introduction, light is basically an electromagnetic wave. For a single frequency, this wave can be represented by a cosine function:

$$I(t) = I_o \cos(2\pi\omega t)$$ (Equation 1)

Where ω represents the frequency of the wave and I(t) is the amplitude of the wave after time t. As with any wave, it can experience interference from another wave of the same frequency, both constructive (when the waves are totally in phase) and destructive (when the waves differ by ½ a wavelength). Schematically (Figure 5):



Destructive interference (1/2 wave phase difference) Constructive interference (waves in phase)

Figure 5. Destructive and constructive interference

To achieve this interference, a device called a Michelson Interferometer is employed. The device is named after the previously mentioned Albert Michelson, who received the Nobel Prize in Physics in 1907 "for his optical precision instruments and the spectroscopic and metrological investigations carried out with their aid". One of his major research projects was measuring the speed of light by reflecting a beam of light between Lookout Mountain and Mt. Wilson in California in 1920, essentially refining an experiment he devised at Annapolis in 1879. He was able to measure this constant to an accuracy of 0.004%!

In a Michelson Interferometer, a collimated beam of light is incident upon a beamsplitter; an optic which partially reflects the light and transmits the remainder to create two beams of light. One beam is sent onto a fixed mirror, and the second beam is sent onto a moving mirror assembly. These two beams are then recombined at the beamsplitter causing the aforementioned interference. As the moving mirror is operating, the distance that one beam changes, bringing that beam into and out of phase with the beam from the fixed mirror. This "optical retardation" creates the interference pattern, which can be observed with an optical detector; the result is an oscillating signal:

$$I(\delta) = 0.5\, I\,(\acute{\upsilon}_o)\cos 2\pi\acute{\upsilon}_o\delta \qquad \text{(Equation 2)}$$

Where I($\acute{\upsilon}_o$) is the intensity of the light source at frequency $\acute{\upsilon}$ and δ is the mirror displacement, which is a multiple of the wavelength of the light. This is an equation for a single frequency interferogram. Schematically (Figure 6):

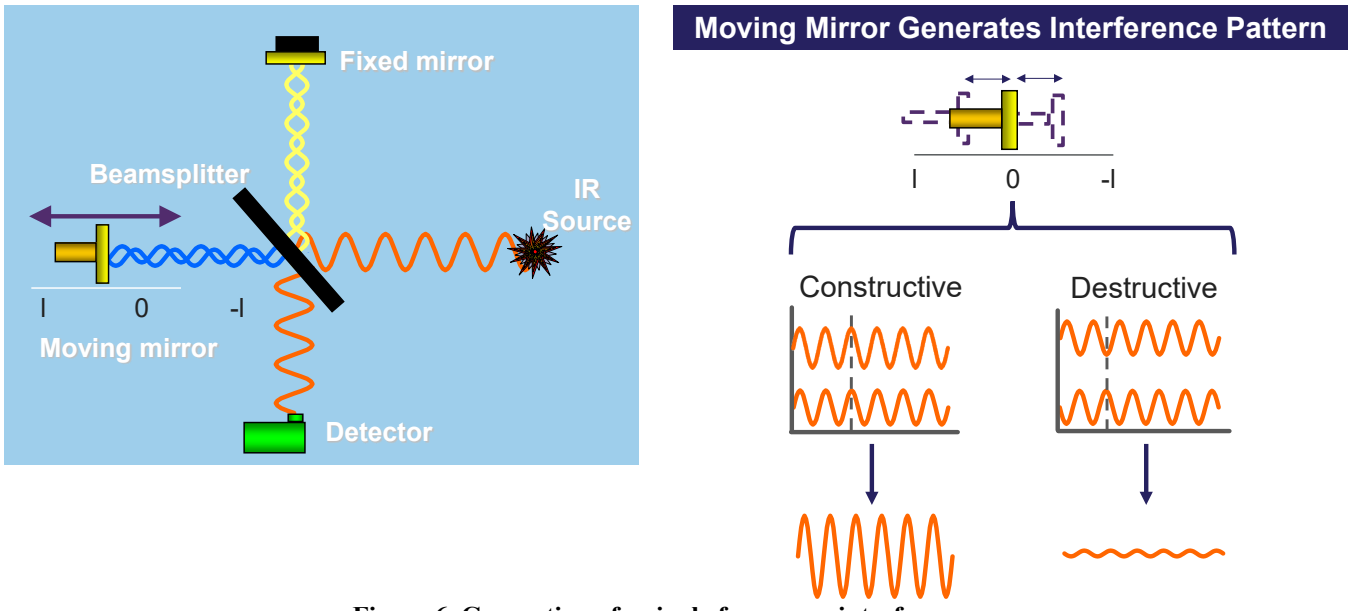


Figure 6. Generation of a single frequency interferogram

In reality, the IR source is not one frequency but a continuum of frequencies, all with individual cosine dependencies and intensities. In this case, Equation 2 becomes:

$$S(\delta) = \int_{-\infty}^{+\infty} B(\acute{\upsilon})\cos 2\pi\acute{\upsilon}\delta\, d\acute{\upsilon}$$

and (Equation 3)

$$B(\acute{\upsilon}) = \int_{-\infty}^{+\infty} S(\delta)\cos 2\pi\acute{\upsilon}\delta\, d\delta$$

These equations are the cosine Fourier Transform pairs (named after mathematician Joseph Fourier) between what is known as the Interferogram $S(\delta)$ and its spectral distribution $B(\acute{\upsilon})$, also known as the single beam spectrum. This is the "FT" in FTIR and is the fundamental basis for the technology. The electrical signal created with a broadband continuum source is shown in the following diagram:

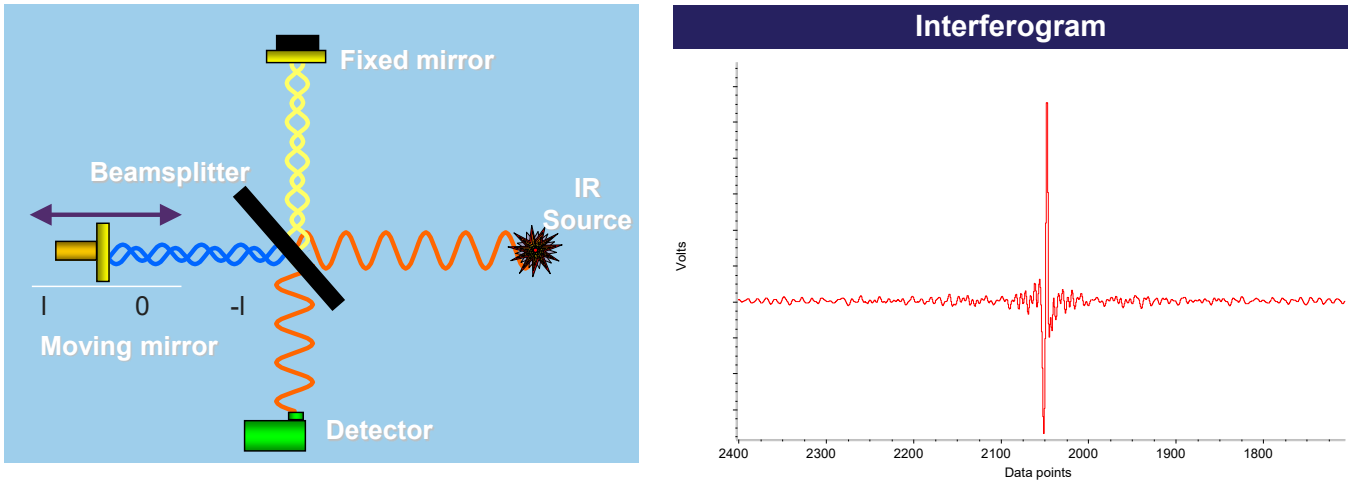


Figure 7. Generation of a broadband interferogram

The first thing one notices is that there is a sharp feature in the center of the interferogram. This is when the distance between the fixed mirror and the beamsplitter is exactly equal to the distance between the moving mirror and the beamsplitter. This is called the "centerburst" or ZPD (for zero path difference). In addition, the interferogram should be totally symmetrical about ZPD; in reality it is not, but there are ways that the mathematics can clear up this "phase difference". Also, the small oscillations which are seen after ZPD and out to the ends of the interferogram are extremely important since they carry the majority of the spectral information. In fact, as the moving mirror is moved farther and farther out from ZPD, the resolution of the FTIR (the ability to see narrow spectral features) becomes sharper and sharper. Typical resolution on a commercially available FTIR is on the order of 0.5 to 1 cm^{-1}. So now that we see how an interferogram is collected, how do we get to the final infrared spectrum?

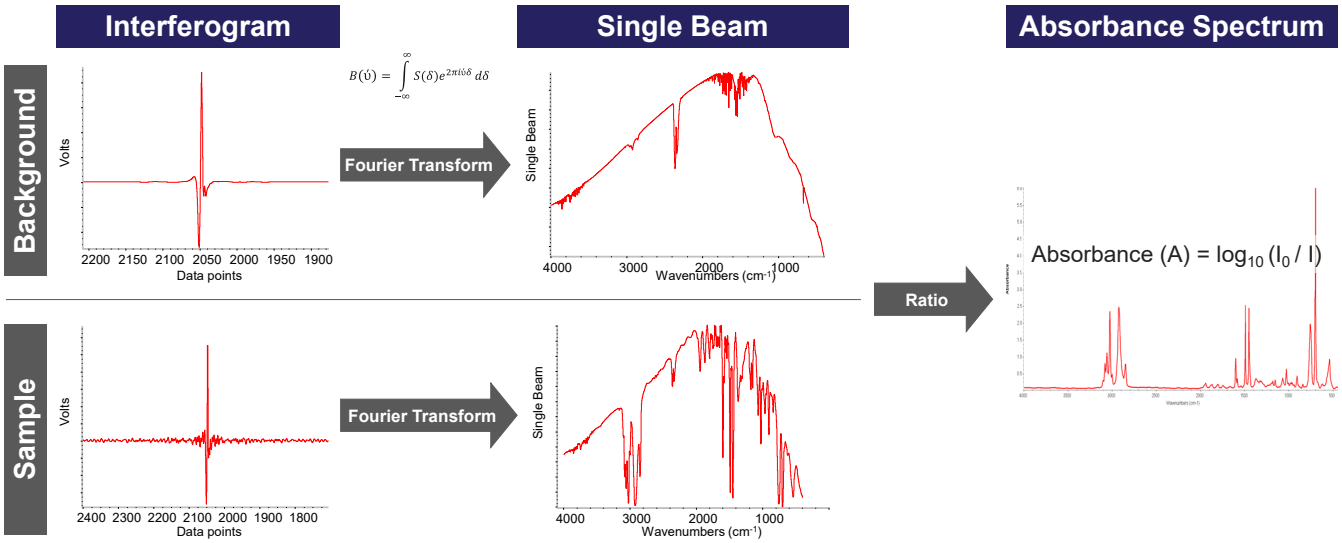


Figure 8. Process for generating absorbance spectrum

The first step is to record the interferogram of an "empty" gas cell; in this case the cell is not empty but contains one of the infrared "invisible" gases we mentioned earlier (usually purified nitrogen or clean, dry air). This is transformed into the single beam "background". Next, we run the gas sample of interest into the same cell, displacing whatever background gas was in there. The interferogram and single beam are recorded in the same manner. Just as in any form of optical spectrometry, the recorded absorbance follows Beer's Law:

$$A = \log_{10}(I_o/I) \quad \text{(Equation 4)}$$

Where I_o is the background single beam intensity, and I is the sample single beam intensity. The implications of Beer's Law and subtle deviations from it will be discussed later on.

Advantages of FTIR

From this overview of interferometry, one can see that there are very significant advantages over the original dispersive spectrometers that directly relate to the sensitivity enhancement facilitating the detection of very low gas phase concentrations. Among which are:

Fellgett's (multiplex) advantage

This advantage arises from the fact that all of the light is being detected simultaneously in an interferometer rather than one spectral element at a time as in a grating spectrometer. The signal-to-noise ratio (SNR) increase of this interferometric measurement over that of a grating spectrometer goes as the square root of the number of spectral resolution elements $(N)^{½}$. In this case, to measure a dispersive spectrum with the same SNR as an interferometric measurement requires N times longer duration. For example, a standard mid-infrared measurement with a spectral bandwidth of 3,600 cm^{-1} and a resolution of 1 cm^{-1} would take a grating spectrometer 1 hour to acquire what could be performed in one second on an FTIR!

Jacquinot's (throughput) advantage

Reviewing the diagram for the dispersive infrared spectrometer, there are two major apertures in this design. The first is the entrance slit, which creates a virtual point source for a lens to create a collimated beam to impinge the grating or prism such that the image is retained after being dispersed. The collection lens then can reform a spectrally distributed point source at the exit slit. As the grating or prism is rotated, each spectral element passes through the exit slit and onto the sample. Obviously in this design, >99% of the useful light is blocked and not detected at any one time. The calculated throughput depends upon the slit size, illuminated area of grating and focal length of the lens system. Since there is no need for slits in an FTIR, the only determining factor is the size of the beam traversing through the beamsplitter. In comparison to a typical grating spectrometer, an FTIR provides a 50-500x advantage

Connes (frequency precision) advantage

Since the basis for measuring the mirror displacement (and hence the frequencies of the light measured through Equation 3) is a laser (which has a very narrow emission bandwidth and a long coherence length) the precision of the measured frequencies is typically ±0.01 cm^{-1} or less. This is to be contrasted with a grating spectrometer, which uses an encoded gear drive to determine the angular change in the prism or grating and is subject to gear slippage, sticking, etc. which can directly affect the accuracy of the light being measured. In earlier days, a standard material, such as indene liquid or polystyrene film would be used to validate wavenumber accuracy. Typically, with FTIR one isolated water band (with a published frequency known down to 0.0001 cm-1) is used to compare to the observed band. The information allows the calculated laser frequency to be mathematically adjusted to agree down to this precision.

Stray light advantage

In grating spectrometers, as the light passes through the sample and onto the detector, it creates a DC current which is converted to a voltage proportional to the flux of the light incident. Since the signal is DC, a great deal of engineering had to go into baffling any other light which may "leak in" and be detected. Long blackened channels of metal shrouding were used to minimize this. In FTIR, the interferogram is naturally an AC measurement since the interference pattern intensity oscillates as the mirror moves. In this way optical frequencies produce a signal in the range of audio frequencies and a low pass filter can block out any DC component, so any continuous background signal (stray light) is eliminated.

Standard Layout of an FTIR

Although there are minor differences between FTIRs, such as the design of the interferometer (corner cube mounted on a voice coil, rocking mirror, double pendulum, etc.), laser (helium-neon laser, diode laser), infrared source (ceramic carbide, Globar, nichrome wire coil, etc.), detectors (mercury cadmium telluride (MCT), deuterated triglycine sulfate (DTGS),

bolometer, etc.), all basically comprise the same task; to acquire the interferometric signal which is mathematically converted into a useable spectrum. The general layout is shown on the following figure:

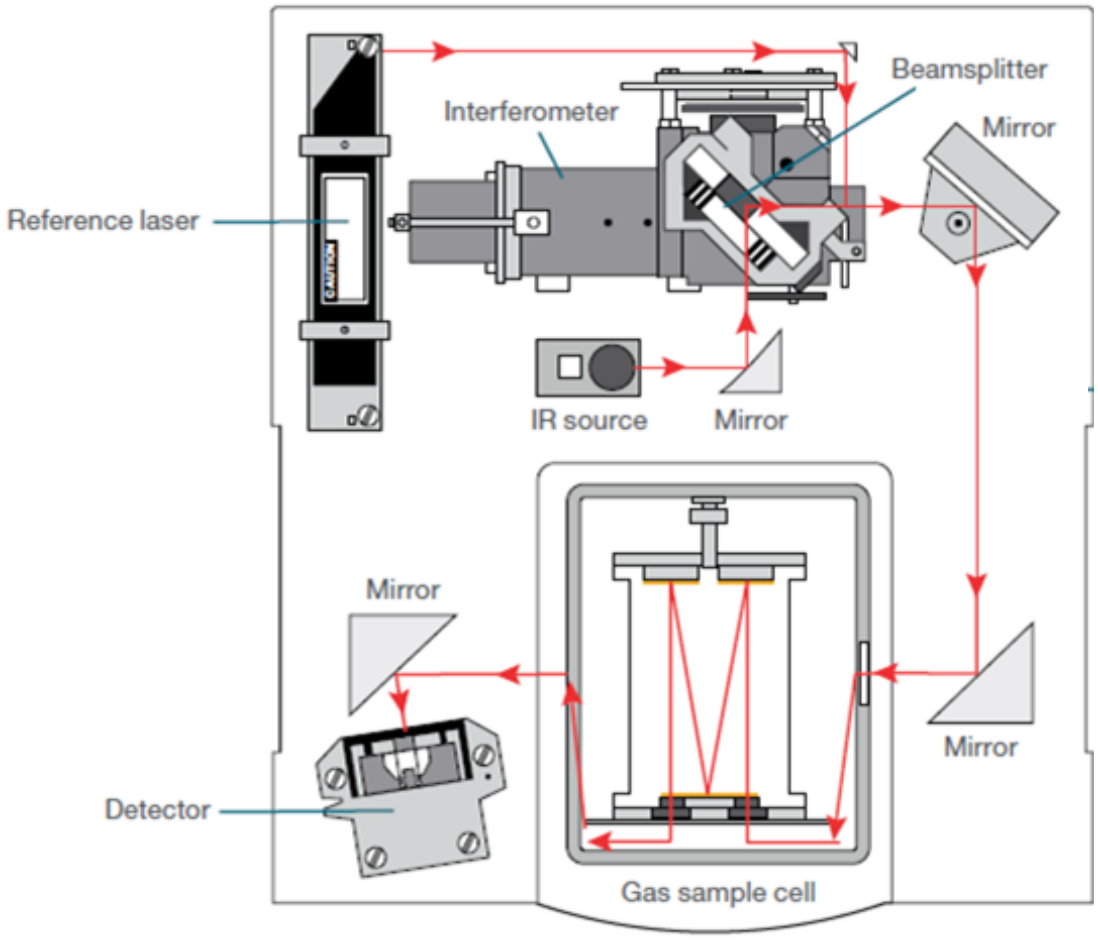


Figure 9. Components of a FTIR

Laser The reference laser is synchronized with the mirror movement to produce a pure sinusoidal wave as it is combined in the interferometer; the modulated laser light is typically sampled at 2 points, known as the zero crossings. In some cases, the laser beam is optically "doubled" by using a ¼ wave plate, providing 4 zero crossings. Knowing the precise position of these crossings reveals the precise positioning of the moving mirror and hence the precise retardation used for the Fourier Transform to frequency. Helium-Neon (He-Ne) lasers provide a perfect reference source; however, they are relatively large and have a limited lifetime due to the laser-active gases gettering out to the tube walls. Newer commercial models now use vertical cavity surface emitting lasers (VCSELs) which are diode lasers a fraction of the size of He-Ne lasers and have a lifetime of 10+ years before replacement.

Interferometer In the interferometer, we have the aforementioned moving and fixed mirror assemblies. The beamsplitter is made from infrared transmissive or partially transmissive material substrates (potassium bromide, zinc selenide, germanium) which have a vapor deposited coating to ideally create a 50/50 transmitting/reflecting situation. A disadvantage of using potassium bromide as the substrate is the fact that it is hygroscopic and requires a dry purge gas or desiccants to maintain low humidity within the interferometer.

IR Source As mentioned previously, the IR source is typically a resistively heated ceramic maintained at a temperature of 1000-1500º C, which has an emission bandwidth from 500-8000 cm^{-1}; this light is collimated and directed into the interferometer using a parabolic reflector.

Gas cell The light leaving the interferometer is then directed into the gas sample cell. The gas sample cell is an optically sealed set of mirrors with infrared transparent windows which allow the light to enter and leave. The mirrors are sealed onto the cell body using compression O-rings, usually made from fluorocarbon materials such as Viton™ or Kalrez®. The cell body is typically constructed from aluminum or stainless steel and is sometimes coated with nickel plating or is electropolished for a smooth internal surface. There is tubing which is either welded or attached with fittings to allow for the gas to flow in and out of the cell with sufficient mixing to get a true measure of the gas composition. The mirrors are typically gold coated and are designed such that there are three concave spherical mirrors with identical radius of curvature where the mirror separation is equal to the radial distance . This forces the entrance beam to reflect back and forth between the mirrors with a slight shift in position with each reflection; this design is typically known as a "White cell" (named after the inventor). Using this multi-reflective cell creates an effective pathlength which can be multiple meters long. The pathlength will be discussed in the following section on the analytical measurements for gas concentration.

Detector After the beam has passed through the gas cell, it is directed onto the infrared detector. As mentioned, there are various detectors which can be used, each with their own strengths and weaknesses. Mercury-Cadmium-Telluride (MCT) detectors are one of a group of semiconductor photonic detectors. The composition of the MCT determines what is known as the bandgap or energy difference between the ground and conductive states of the semiconductor. When a photon of the correct energy impinges on this detector, it forces an electron up into the conductive state and this electron forms the current that is detected. These photonic detectors are very sensitive and very fast; essentially, 1 photon = 1 electron. They are also operated at cryogenic temperatures through the use of liquid nitrogen or thermoelectric cooling. The problem arises at very high light fluxes, where the bandgap transition can get saturated and therefore the observed signal becomes highly nonlinear. In this range, observed absorbance response is dramatically unrelated to analyte concentration. Some groups have successfully developed mathematical or electronic corrections to this response curve to artificially "linearize" them. The second class of detectors are pyroelectric detectors, among which is Deuterated Triglycine Sulfate (DTGS). This detector works on the principle that when infrared light is absorbed by this material, it heats up and its crystal lattice deforms (expands) slightly, causing a charge separation on the surface of the crystal lattice. This charge separation is the source of the current which is measured. Since the basis of this process is not a direct photonic one, this type of detector is not as sensitive nor as fast as a photonic detector, which requires that the moving mirror modulation must be slower and hence the overall data rate is slower. However, these detectors do not have the same susceptibility to saturation and hence are very "linear" detectors. Another advantage is that they are operated at room temperature; no cooling is necessary.

A/D Digitization and Computation The voltage generated by the detector current is then collected and digitized using an analog-to-digital converter. Each voltage level is represented by a bit pattern in which as the higher the voltage rises, the more significant bits are set. Each sample analog voltage measurement has its own pattern of bits which is interpreted by the computer's CPU as the respective voltage level. Modern A/D's have between 18- and 24-bit capabilities which allow for large dynamic range measurements, especially considering that an interferogram has a wide gap of voltage between the centerburst and the small oscillations out at large mirror displacement (where the higher resolution spectral information occurs). Now we can also see why FTIR is only a relatively recent spectral invention (the first commercial FTIR was introduced in 1969); the computational power required to perform a Fourier Transform was not practically available until then. Fortunately, Fourier Transforms have some very valuable symmetrical properties that allow matrix solutions to be performed nearly instantaneously; these are called FFT (for Fast Fourier Transform) algorithms which have both firmware and hardware 'canned" capabilities.

FTIR Analytics

We have now discussed the principles of interferometry and Fourier Transforms, but how does this translate into a viable analytical technique for gas analysis?

As shown previously, the Interferogram (I-gram) is collected for an "empty" cell (N_2 gas) and is Fourier Transformed into the single beam (S-beam) representation of the light intensity vs. frequency. The same procedure is then done for the gas sample such that we end up with two S-beams that are then ratioed to one another and logarithmically converted to absorbance

versus wavelength as diagrammed in Figure 8. There are a few steps to be discussed to get from this absorbance calculation to actual concentration results which contain subtleties that must be considered to ensure accurate results.

A major result of the multiplex advantage is that the entire infrared spectrum is calculated at once, so all infrared active gases can be detected simultaneously, whereas a technique such as Gas Chromatography detects each gas separately as it is eluted from the column. Thus, FTIR can significantly decrease analysis time for a gas mixture. For example, a resultant spectrum for a multiple gas mixture can look like the following (Figure 10).

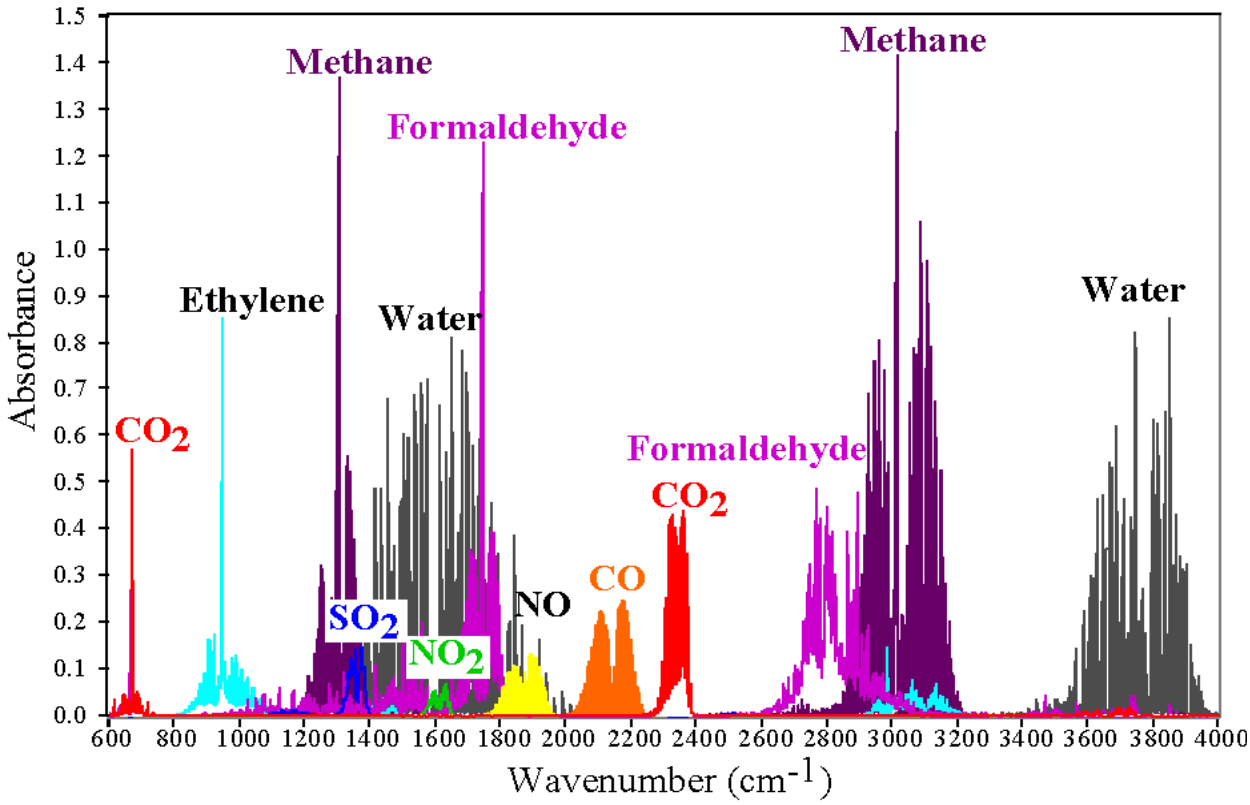


Figure 10. Multiple gas mixture example

Each gas in this mixture has a unique spectral signature which is determined by Quantum Mechanics; the vibrational potential energy surface for each type of motion is fixed such that for a fixed temperature, pressure, bulk matrix gas and operating parameters of the FTIR, the spectrum is immutable. By designating particular spectral features for each gas as a marker for its concentration (called the quantification region or "quant" region), we can independently analytically determine each gas in the mixture. There are some critical steps to this process which will be discussed further.

As mentioned before, optical spectrometry is controlled by Beer's Law, which was described in Equation 4. However, it must be noted that absorption is spectrally dependent, so a more proper description of Equation 4 is:

$$A(ú) = \log_{10}[I_o(ú)/I(ú)] = \varepsilon(ú)bC \quad \text{(Equation 5)}$$

Where ε(ú) is known as the molar absorptivity and is frequency dependent, b is the pathlength which the probe beam traverses (i.e., the total pathlength of the multiple reflections mentioned earlier) and C is the concentration of the gas analyte. This is the equation for one analyte, however in a multi-component mix such as shown in Figure 10 where more than one component can absorb at frequency ú, we need to sum over all components (in this case, N components):

$$A(ú) = \sum_{i=1}^{N} \varepsilon_i(ú)bC_i \quad \text{(Equation 6)}$$

Another facet of gas phase spectra analysis which directly affects the apparent molar absorptivity and hence the overall absorption and calculated concentration are the operating parameters of the FTIR. In particular, there are two main settings

which can affect the band shape and thus the absorptivity. They are the resolution of the FTIR and the apodization function of the FTIR which will be discussed here:

Resolution/Apodization As previously discussed; the I-gram is the resultant signal from the integration of all of the cosine dependencies for all emitted frequencies of the infrared source. In an ideal world the integral is over an infinite mirror displacement δ as in Equation 3. However, this cannot happen in reality, so the transform has to be truncated over a defined displacement distance. In the extreme we are multiplying (convolving) the infinite integration with a step function ("boxcar") that has a width of ±Δ, where Δ is the limit of mirror movement in the interferometer. For a single monochromatic line, the resultant spectral curve is a sin(x)/x or sinc(x) function whose baseline width is 1/Δ. This is called the ILS or instrument line shape function. This function also has the property of excursions below the baseline as well. Graphically:

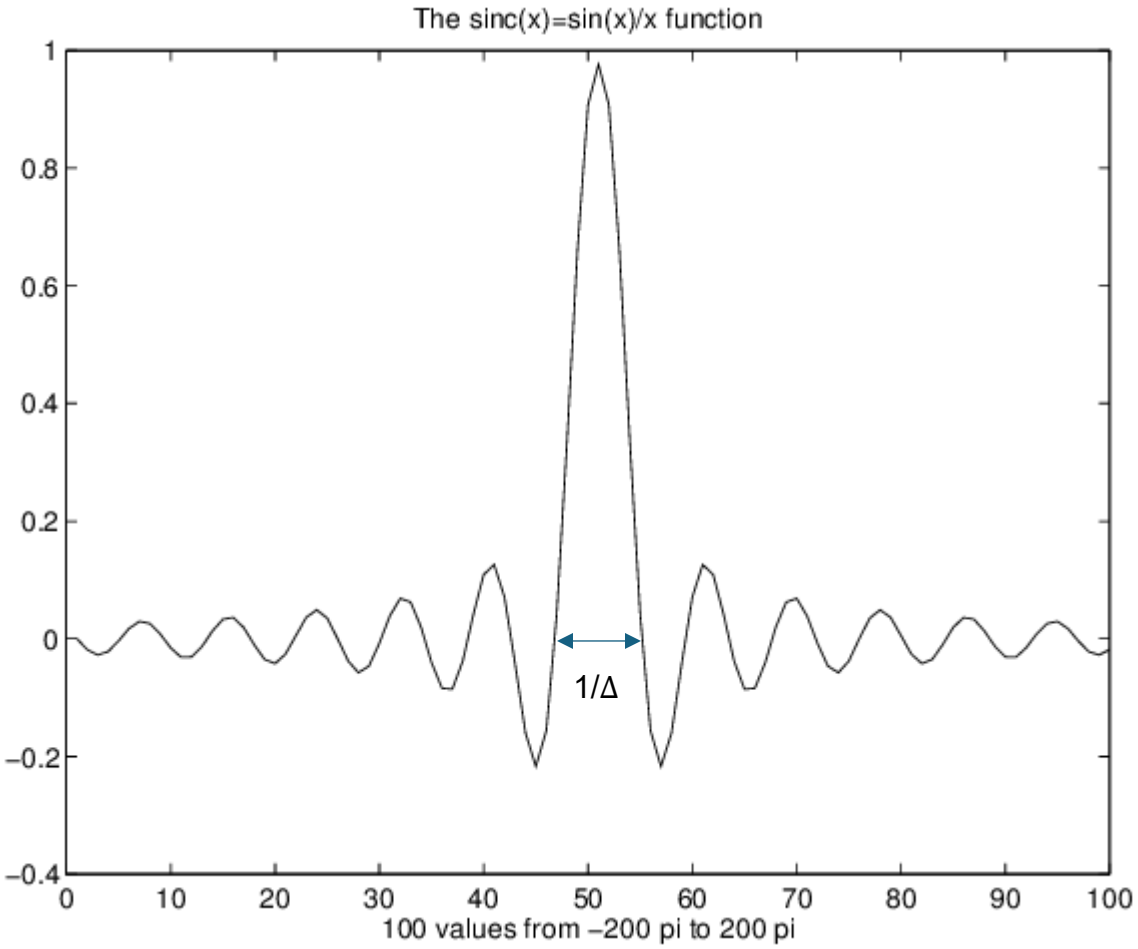


Figure 11. sinc (x) function

So, two monochromatic lines separated by $(\Delta)^{-1}$ cm^{-1} would be completely resolved. However, the oscillations beyond the main $(\Delta)^{-1}$ cm^{-1} width cause noise in the measurement. So rather than utilize a boxcar function, other functions which have a gentler transition down to finite displacement are used. These functions are called apodization functions (apodization literally means "remove the feet"). There are many functions which have been used for apodization- triangular, Bessel, trapezoidal, cosine, etc. Each has their own effect on the observed spectral resolution and noise suppression in the final transform. One of the more common apodization functions used which has been researched to have the best adherence to Beer's Law was developed by Norton and Beer. One important fact from the effect of apodization; no matter which one is chosen, it MUST be maintained throughout the entire analytical process, since the overall spectral lineshape and resolution are directly affected by apodization.

Calibration In order to accurately assess the concentration of a gas (or any analyte for that matter), a comparison of the observed absorption of the gas to a known certified standard gas must be performed. In the case of gases, what is typically

done is that a certified blend of a simple component gas diluted in an infrared transparent bulk gas (usually nitrogen or clean, dry air) is further diluted by a precisely controlled gas divider, in which a fraction of the certified blend is ratioed down in concentration with a known amount of pure bulk gas. This procedure creates multiple concentration levels of the single component gas, each of which has their infrared spectrum recorded. A plot of the observed infrared absorption versus the calculated concentration is the calibration. A single peak absorbance is rarely used for the calibration, rather an integrated area of the absorption over the selected quant region. Ideally, according to Equation 6, this should be a linear plot. In reality, there are factors which cause deviation from this ideality. Instrument manufacturers represent this plot in alternate but equal ways, either as a plot of the integrated absorption vs. concentration or a plot of the apparent concentration (corrected for temperature and pressure) using a scaled representative spectrum within the calibration set vs. the calculated concentration of the other members of the set using this representative. The best fit using a Taylor expansion is utilized to interpolate for any concentration within the span of the plot. The main cause for nonlinearity in gas phase calibration plots has to do with the ratio of the resolution of the apodized spectrum to the actual linewidth of the infrared transition (called the resolution parameter). In effect, there is a deviation between the true absorption and the measured absorption. The un-apodized transmittance ILS is what is first measured by the detector and as concentration increases, the calculated integrated absorbance (after logarithmic conversion from transmittance) increases not only at the peak, but also in the wings since the resolution parameter is not infinitely small and can track the true peak absorbance correctly. In effect, the lineshape deviates from a Lorentzian and "grows" side lobes or wings. This normally occurs for concentrations where the peak absorbance is > 0.7. We can show this graphically. In Figure 12, we show the quant region for a relatively "heavy" gas molecule 1,3,5-trimethyl benzene. Its line width is on the order of 20 cm^{-1} (with an apodized resolution of 0.5 cm^{-1}, we have a resolution parameter of 1/40 or 0.025). In this case, the plot is linear over 3 orders of magnitude in concentration (Figure 13).

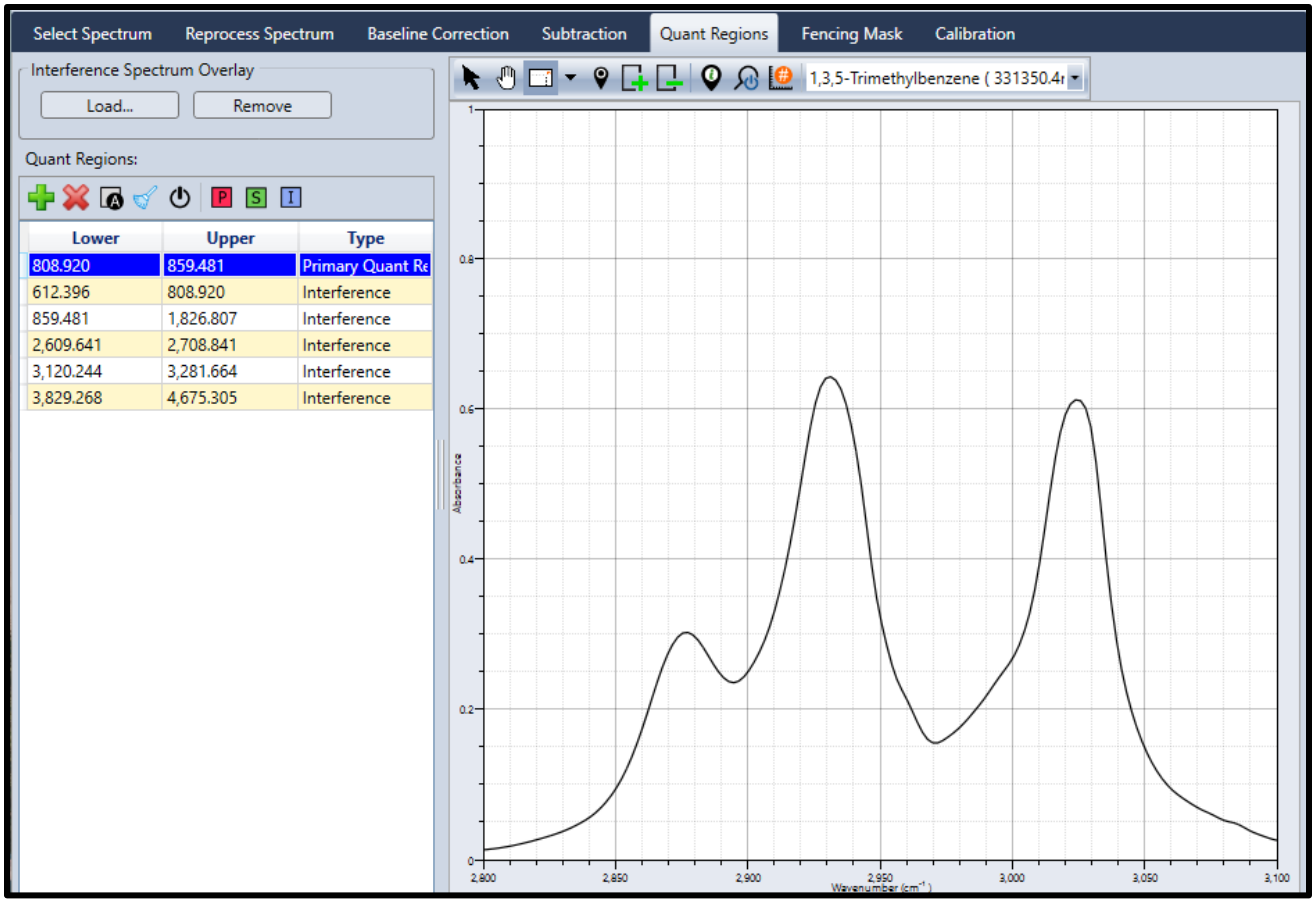


Figure 12. Quant region for 1,3,5-trimethyl benzene

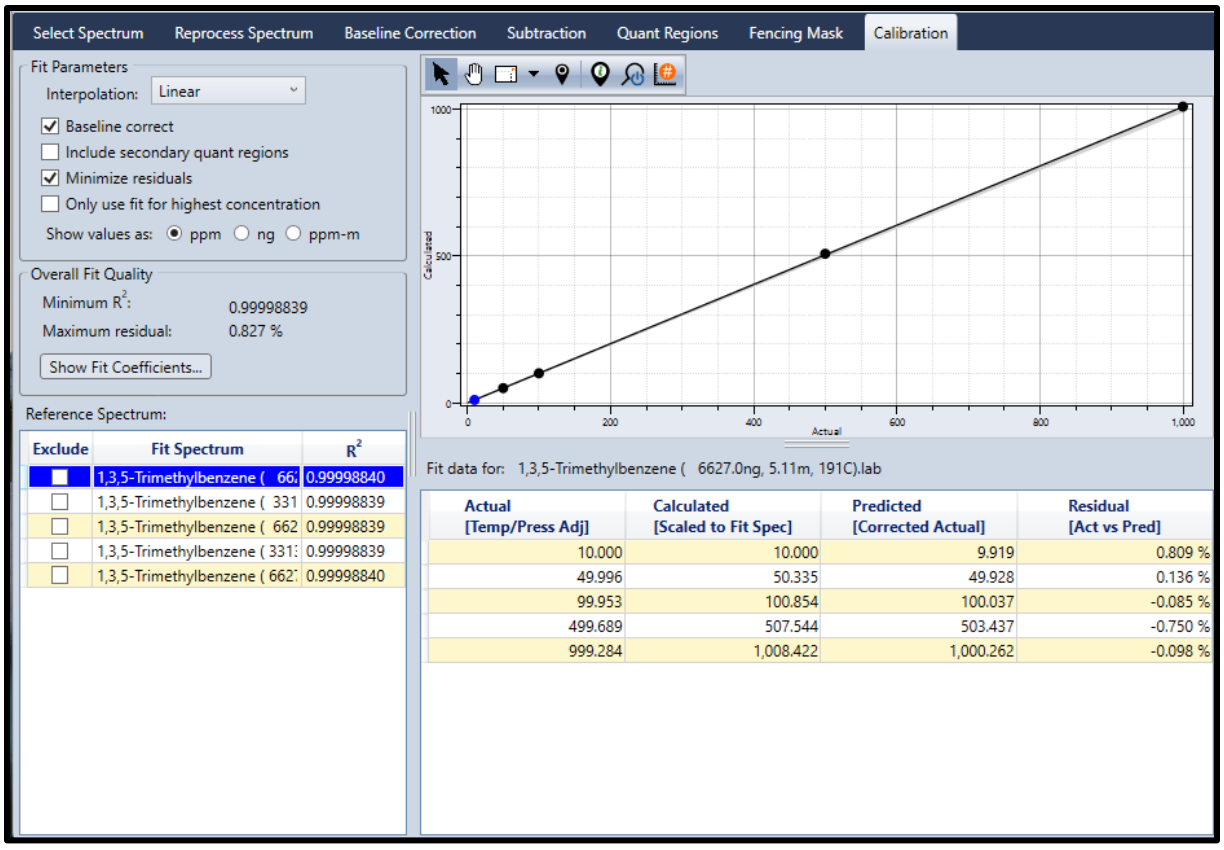


Figure 13. Concentration plot of 1,3,5-trimethyl benzene

Now, we compare and contrast that to a "light" molecule, in this case carbon monoxide, CO. This molecule's only fundamental vibration has noted rotational sub-bands around 2000 to 2250 cm^{-1} of which a small section is shown (Figure 14).

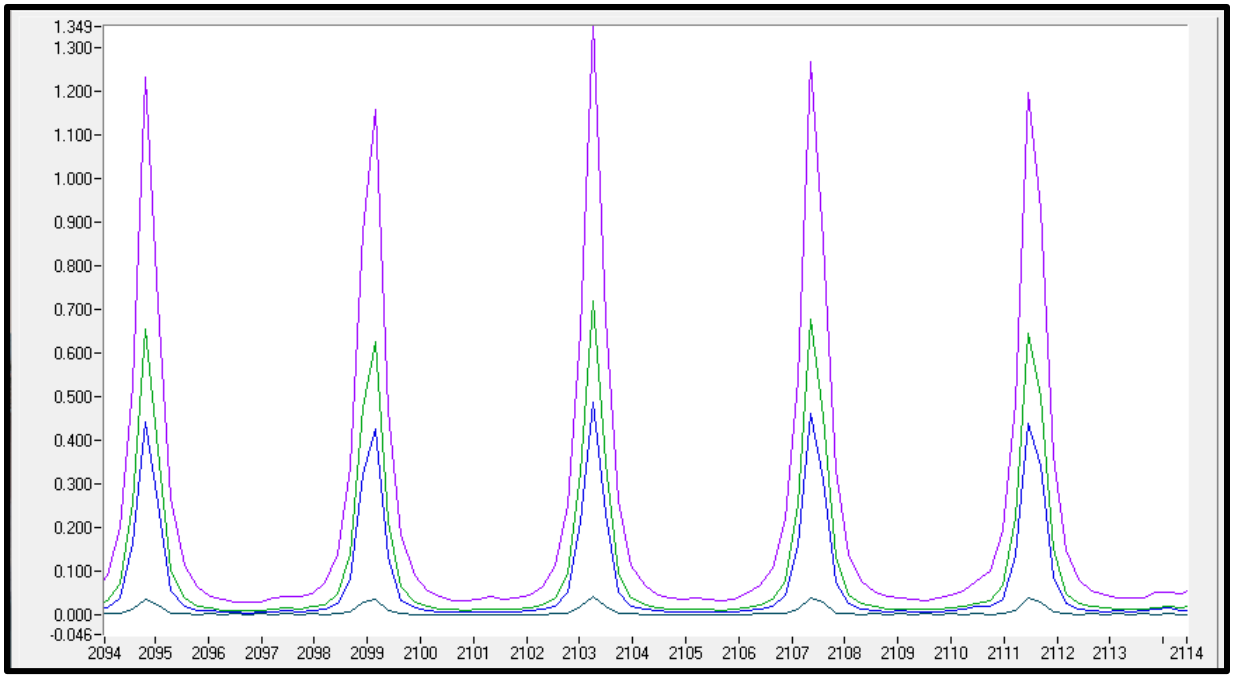


Figure 14. Vibration-rotation bands of carbon monoxide

In this case, the natural linewidth of these transitions is a fraction of the resolution, such that the resolution parameter is much greater than one. As the concentration of the CO is increased and the observed absorbance is ~1.2, it is apparent that the lobes or wings are increasing at a faster rate than the central absorbance, resulting in a negative deviation in the concentration plot as shown in Figure 15.

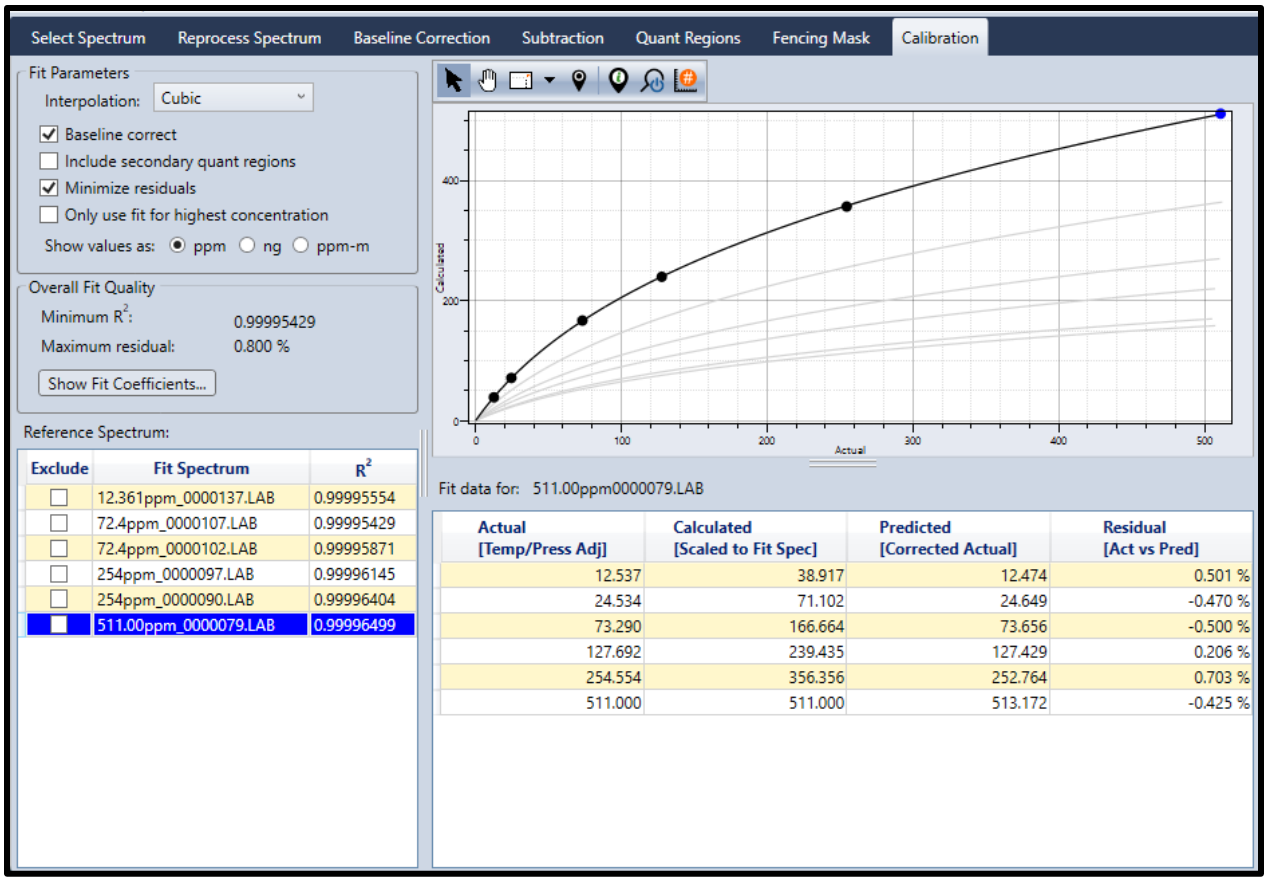


Figure 15. Concentration plot for carbon monoxide

Now, as long as the instrumental parameters are kept constant for the calibration as well as the actual analysis, this curve will not change and is perfectly viable for analysis. In many cases, there is the availability of overtones or weaker bands whose smaller absorption results in less Beer's Law deviation. In addition, as concentration approaches very low levels (low ppm and ppb) the concentration plot naturally approaches linearity for this same reasoning.

Once calibration curves are calculated for the gases of interest, a method is created using these gases. The method is used to fit the observed overall spectrum with resulting calculated concentrations for each gas. To do this we use a classical least squares algorithm.

CLS Method In the simplest case, we assume 2 noninteracting gases (x and y) in a mixture which have some overlap. For this situation, the absorbances of each component add together. Since the two components will have differing spectra, there must be at least two wavenumbers where the concentrations can be seen to vary, we will designate them as $\acute{\upsilon}_1$ and $\acute{\upsilon}_2$. The absorbances at these two wavenumbers are:

$$A_{\acute{\upsilon}1} = \varepsilon_{x,\acute{\upsilon}1} b C_x + \varepsilon_{y,\acute{\upsilon}1} b C_y + E_{\acute{\upsilon}1}$$

and (Equation 7)

$$A_{\acute{\upsilon}2} = \varepsilon_{x,\acute{\upsilon}2} b C_x + \varepsilon_{y,\acute{\upsilon}2} b C_y + E_{\acute{\upsilon}2}$$

Where ε, b and C were defined in Equation 6 and the E's refer to the residual error from this regression at the individual wavenumbers. Since the pathlength b is constant for a fixed pathlength gas cell (the "White" cell mentioned previously), Equation 7 can be re-written as:

$$A_{\nu 1} = k_{x,\nu 1} C_x + k_{y,\nu 1} C_y + E_{\nu 1}$$

and (Equation 8)

$$A_{\nu 2} = k_{x,\nu 2} C_x + k_{y,\nu 2} C_y + E_{\nu 2}$$

Where k is the absorption coefficient (the product of the molar absorptivity and the pathlength). The problem here is that we have two known quantities (the absorbances) but 4 unknown quantities (the absorption coefficients). In order to solve this equation, we need to measure absorbances at two other concentrations of Cx and Cy. In this case we have reached what is known as a "singularity", such that the equations are exactly fit, and the residual errors must be zero. This is not an acceptable situation, and many more concentrations should be measured to better calculate the k's. Rather than write a whole series of equations with differing concentrations and absorbances, we can use matrix notation to represent the salient terms:

$$\mathbf{A} = \mathbf{K} \cdot \mathbf{C} + \mathbf{E} \qquad \text{(Equation 9)}$$

Here **A** represents the matrix of absorbances for the two gases at the two wavenumbers, **B** is the matrix of the absorption coefficients, **B** is the matrix of concentrations and **E** is the matrix of residual errors. In actuality, there is no restriction to the number of absorbances, absorption coefficients, or concentrations for this matrix calculation to work. In fact, **A** is usually represented by the entire spectrum of each component. The only restriction is that the number of absorbances must be equal to or greater than the number of concentrations (or components in the mixture). In order to solve the overall concentration of each component in the gas mixture, one must evaluate the **K** matrix. By removing the error matrix (with the caveat that it still exists in this method), Equation 9 can be rearranged by matrix inversion to get:

$$\mathbf{K} = \mathbf{A} \cdot \mathbf{C}^{-1} \qquad \text{(Equation 10)}$$

Where $\mathbf{C}^{-1}$ is the inverse of the concentration matrix; this is only valid if **C** is a square matrix (i.e., the number of samples is equal to the number of components). Normally, with the Beer's Law calibration plots, there are many more samples than components expected in a gas mixture. In this case, **C** is not a square matrix; its inverse must be calculated from a pseudoinverse using its transpose $\mathbf{C}^T$:

$$\mathbf{K} = \mathbf{A} \cdot \mathbf{C}^T \cdot (\mathbf{C} \cdot \mathbf{C}^T)^{-1} \qquad \text{(Equation 11)}$$

Once **K** is known (from the calibration curves for each component), the concentration $\mathbf{C}_{unk}$ for each unknown can be calculated from the observed absorbances of the unknown gas mixture $\mathbf{A}_{unk}$ as follows:

$$\mathbf{C}_{unk} = \mathbf{A}_{unk} \cdot \mathbf{K}^T \cdot (\mathbf{K} \cdot \mathbf{K}^T)^{-1} \qquad \text{(Equation 12)}$$

This is the basis of classical least squares regression (CLS). There are some distinct advantages using this technique for gas analysis. It is a multivariate technique so there are no restrictions on spectral range and having many samples included in the analysis has a large averaging effect, so the **E** matrix is usually minimized. This **E** matrix represents what is known as the "residual" (i.e., what is left over after the fitting has occurred). There is one disadvantage using CLS in that ALL of the components in the gas mixture must be accounted for and have a calibration model included in the matrix. If this is not done, the overall calculation will be incorrect and typically the **E** matrix will not be randomized "noise" but contain structure to it, reflecting spectral information of the missing component. As also mentioned earlier there can be no secondary interactions (such as hydrogen bonding) which could modify the base calibration spectra. Fortunately for gas analysis, secondary interactions are rarely a problem due to the fact that the gas molecules are widely separated.

For a more detailed explanation behind the theory and instrumental aspects of FTIR, there is an excellent monograph on the subject: "*Fourier Transform Infrared Spectrometry, 2nd ed.*", eds. P.R. Griffiths and J.A. de Haseth, Wiley-Interscience, 2007. (ISBN 978-0-471-19404-0)

REAL WORLD APPLICATIONS

To demonstrate the power of FTIR for gas mixture analysis, a couple of relevant test applications which are now accepted procedures in environmental and process monitoring will be shown next.

Carbon capture, utilization and storage(CCUS) The fight against climate change requires innovative technologies that address greenhouse gas (GHG) emissions, primarily carbon dioxide. CCUS technology plays a critical role, offering a pathway to mitigate emissions from hard-to-abate sectors such as cement, steel, and power generation.

The methodology in which companies capture carbon dioxide varies between industries but can be digested down into four major techniques: pre-combustion, post-combustion, oxy-fuel combustion, and direct air capture. Pre-combustion capture utilizes gasification to produce a CO_2-rich syngas, facilitating easier separation of CO_2. Post-combustion removes CO_2 directly from the flue gas after combustion, typically using chemical solvents. Oxy-fuel combustion burns the fuel in pure oxygen instead of air, producing a flue gas with high concentrations of CO_2. Direct air capture extracts CO_2 directly from the atmosphere, offering flexibility for decentralized emissions sources. Each capture technique presents the potential to introduce various impurities into the captured CO_2 product.

What a facility does with the CO_2 after it is captured is dependent upon the purity of the CO_2 product post-abatement. If the CO_2 product is of high purity, facilities can utilize it to create a sellable product. They can sell the CO_2 directly for use in the food and beverage industry or use the CO_2 as a precursor to create high value solvents such as methanol. If the CO_2 cannot be utilized, the next best option is to transport the CO_2 to a permanent storage location to prevent release to the environment. The CO_2 is liquified and shipped to storage sites with geological formations that are sufficiently porous to allow CO_2 to fill the void.

The absolute purity of captured CO_2 must be monitored continuously to ensure companies receive the government sponsored tax credits associated with offsetting their GHG emissions. The CO_2 must also be monitored and verified that it is within specification to protect company assets in the transportation network.

Monitoring requirements for CCUS present challenges to analytical instrumentation. The systems must have the capability to detect impurities at parts-per-million (ppm) to parts-per-billion (ppb) levels while simultaneously measuring the high percent levels of CO_2 (up to 99.99% +). In addition to a very wide concentration range, the monitoring technology must quantify many different organic and inorganic gases to ensure the CO_2 product is within specification. Instrumentation must operate continuously with minimal downtime and maintenance, and there is also potential for measurement points to be in remote locations where operator intrusion would not be viable, requiring automation.

FTIR has been employed for online analysis for many types of gas streams and is commonly applied to the analysis of beverage grade CO_2. FTIR offers several advantages for the continuous monitoring of CCUS streams. The technology offers a wide dynamic detection range, quantifying gases from ppb to 100%. It collects data in real time, allowing the capture of transient changes to impurity levels. The calibrations are also stable and free of drift, reducing the need for frequent calibration and minimizing downtime.

FTIR was tested for the suitability to monitor impurities within captured CO_2. The targeted impurities were nitric oxide (NO), nitrogen dioxide (NO_2), and sulfur dioxide (SO_2). To ensure that the testing was representative of field data, a simulated stream of ~3500ppm of CH_4 and > 95% CO_2 was used. The inclusion of high concentrations of hydrocarbons and CO_2 tested the specificity of the impurity measurements, ensuring that no interference bias from matrix gases occurred.

The limit of detection (LOD) for each impurity was defined as three times the standard deviation of the measurements for 12 consecutive points in the representative matrix. The measurement time for each data point was 60 seconds. No offsets or span factors were applied to the method. The results are shown in Table 1 below.

Gas	Units	Specification	LOD (3σ)
Nitric oxide	ppm	< 2.5 (NOx)	0.049
Nitrogen dioxide	ppm	< 2.5 (NOx)	0.003
Sulfur dioxide	ppm	< 10	0.082
Water	ppm	< 70	0.406
Acetaldehyde	ppm	< 20	0.002
Ammonia	ppm	< 10	0.011
Carbon dioxide	%	> 95	Matrix
Carbon monoxide	ppm	< 750	0.074
Ethanol	ppm	< 20	0.053
Formaldehyde	ppm	< 20	0.085
Methane	ppm	< 10000	Matrix
Methanol	ppm	< 620	0.075
Nitrous oxide	ppm	NA	0.097
Oxygen	ppm	< 40	1.000

Table 1. Impurity limit of detection (LOD) results

A 14-day drift assessment was performed on the FTIR system with research grade CO_2 (99.9999%) to verify that the CO_2 measurement is stable and free of drift. The results are shown in Figure 16 below.

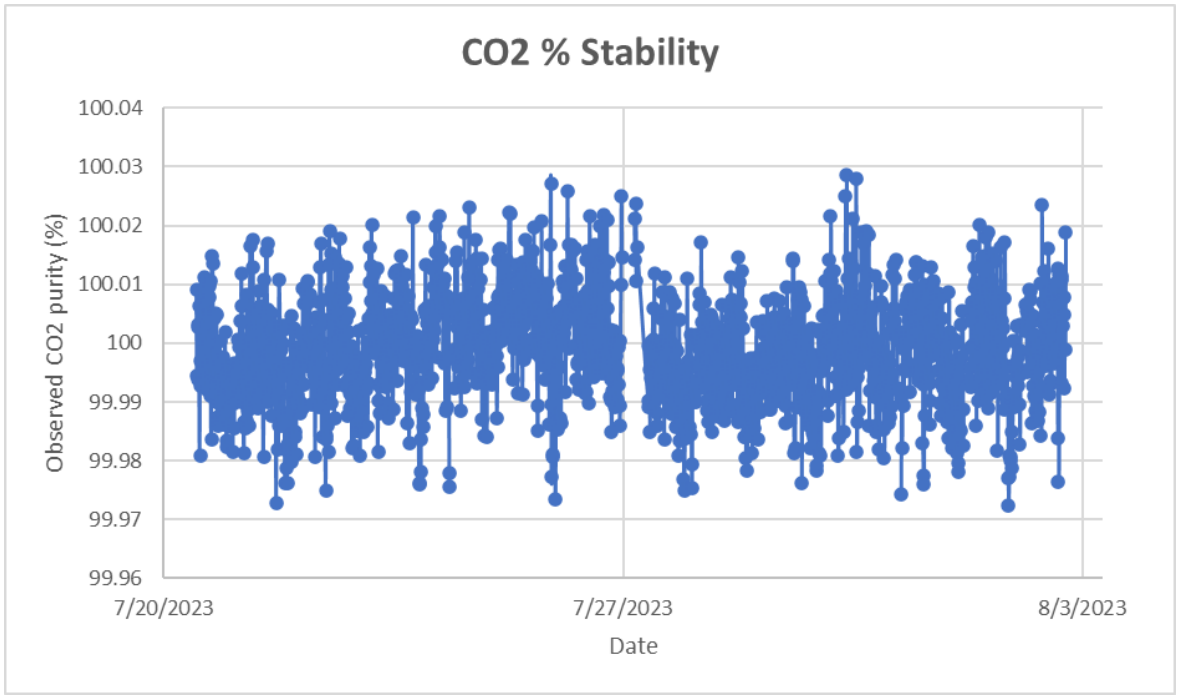


Figure 16. 14-day drift test results on research grade CO_2

Figure 17 shows one of the CCUS test measurements: a mixture of 1200 ppm CH_4 in research grade CO_2. Figure 18 shows the spectrum of beverage grade CO_2 after purification- this sample meets the International Society of Beverage Technologists (ISBT) grade for acceptable impurity levels for soft drink carbonation. In comparing the two figures, it is quite easy to observe the spectral difference between the two samples, especially considering these spectra are collected in a matter of seconds.

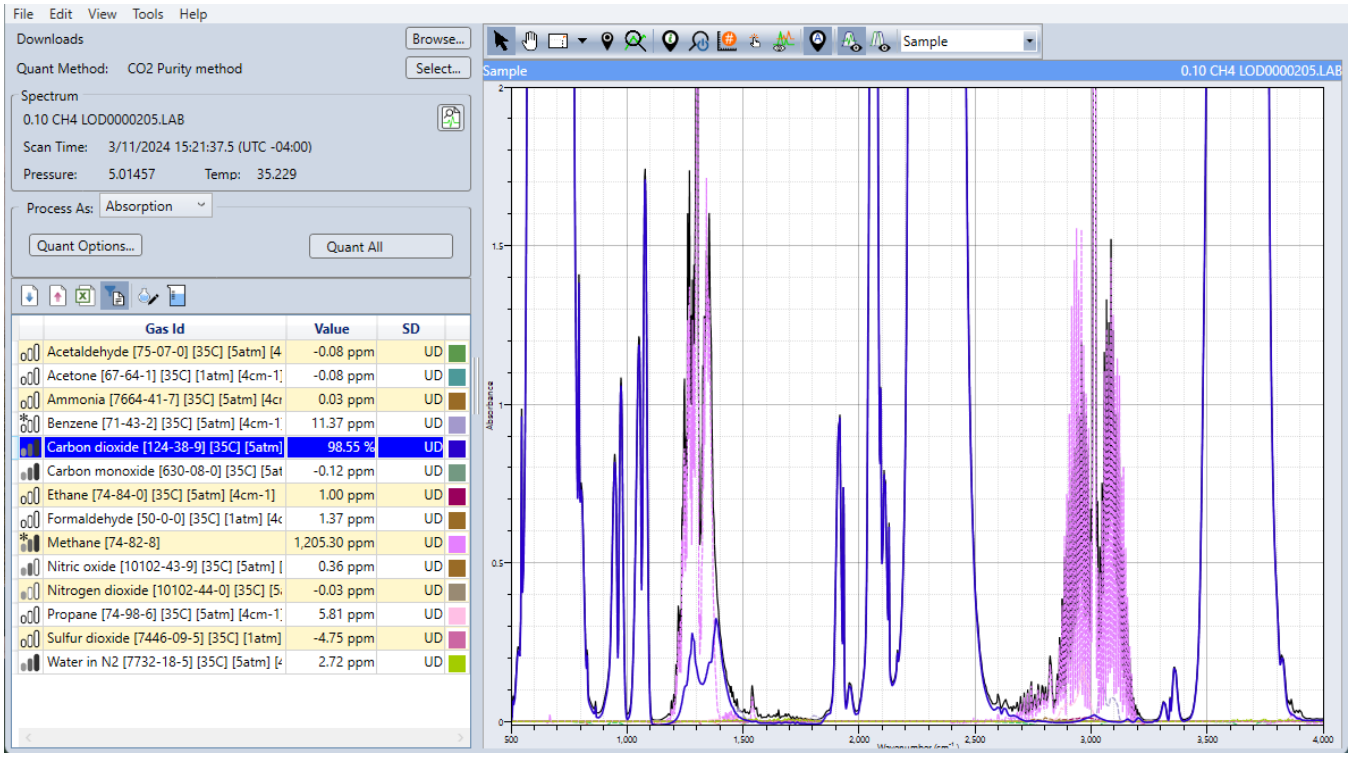


Figure 17. Test mixture of CH_4 and CO_2

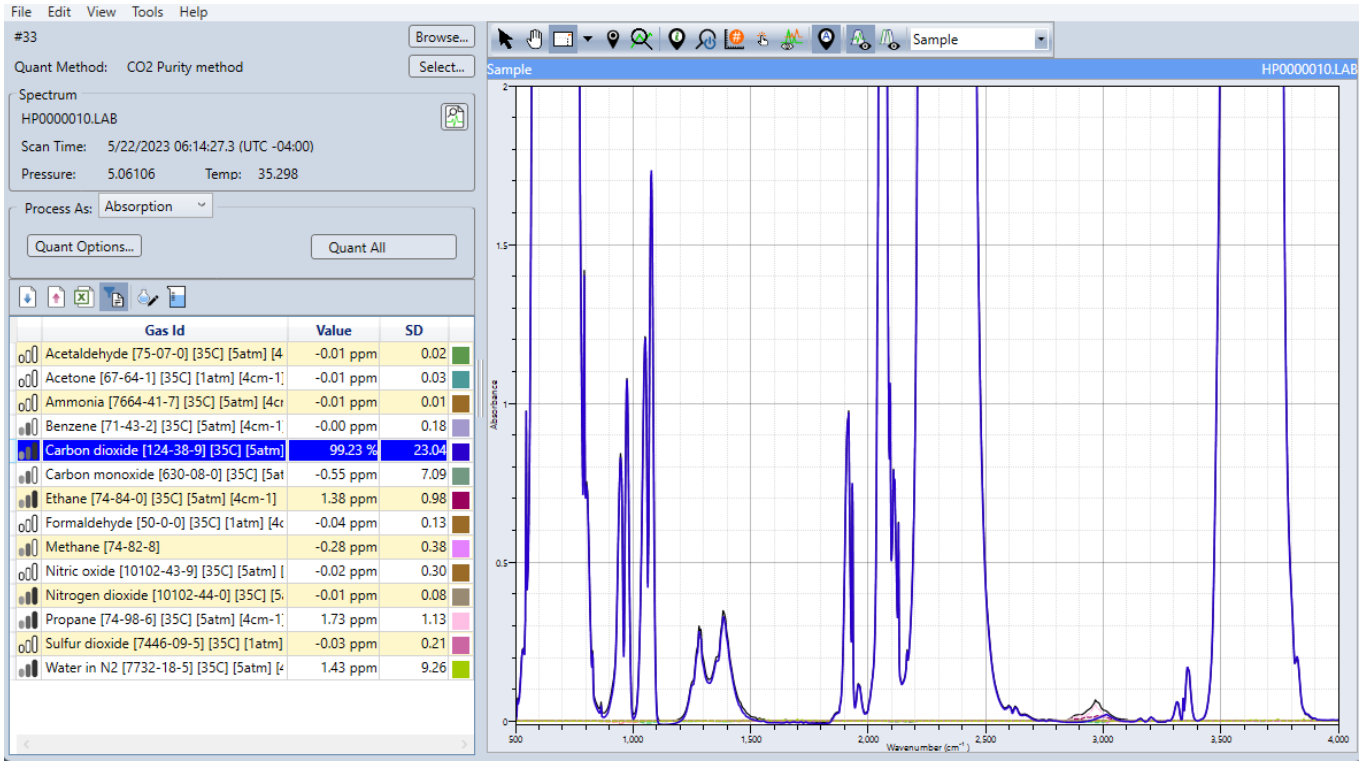


Figure 18. Purified CO2 sample which meets ISBT standards

Measurement of hydrocarbon impurities in oxygen from an Air Separation Unit (ASU) As with any large gas manufacturer, within their arsenal there are a vast chain of ASUs scattered worldwide. These ASUs act as a source for purified bulk gases such as nitrogen, oxygen and argon. To ensure the optimal performance of these ASUs in delivering quality products, the output gas stream must be continuously monitored. For example, hydrocarbons can be present in an air separation unit due to various factors, including feedstock contamination, system leaks and contaminated equipment.

The presence of hydrocarbons in the process can have various implications, such as:

- Hydrocarbons can affect the purity and quality of the separated gases produced by the ASU. Some applications, such as electronics manufacturing or medical gas production, require extremely pure gases with near-zero hydrocarbon contamination.

- Hydrocarbons can impact the efficiency of the ASU process. For example, certain hydrocarbons can act as contaminants that affect the performance and lifespan of process equipment, such as cryogenic systems or separation columns. Controlling hydrocarbon content helps ensure optimal process efficiency and minimize equipment degradation.

- For an oxygen separation process, hydrocarbon contamination and build-up can lead to possibly explosive mixtures being formed

As a result, monitoring of hydrocarbons on sensitive scales (typically ppb levels) is required such that these contaminants are captured and remediated early in the ASU process. Typically, this analysis has been performed using gas chromatography/ flame ionization detection (GC/FID) to detect the specific hydrocarbon impurities. However, there are drawbacks to this technology. Gas chromatographs are notoriously "fickle" instrumentation which need constant human intervention for calibration and maintenance. This is not always optimal since many ASU locations are remote and not easily serviced. In more recent years, FTIR has been used successfully to detect hydrocarbon impurities down to ppb levels in these streams. This has been possible due to the lack of an infrared signature in the bulk gases, hence no large absorption background. The FTIRs which have been commonly used rely on a cooled Mercury-Cadmium-Telluride (MCT) detector due to their very high detection capability. The most sensitive detectors use cryogenic cooling with liquid nitrogen. However, an automated cryogenic supply system or human intervention must be used to maintain the cooling process. Neither option is reliable for remote deployment. Alternatively, thermoelectric cooling of the detector using Peltier devices is sufficient, however, these systems have a reduced infrared bandwidth, so certain regions of the spectrum cannot be probed.

However, as mentioned in the theory section, FTIRs can also use a DTGS pyroelectric detector which operates at room temperature and therefore does not rely on the need for detector cooling yet provides the full mid-infrared range of wavelengths for interrogation of hydrocarbons (as well as other gaseous materials) which could be in a purified bulk gas stream. The FTIR testing involved introducing select impurities at varying levels and combinations. This process was used to determine if there were any interferences which could degrade detection limits and/or sensitivities in such a monitoring process. The primary compound used as the alarm trigger for excess hydrocarbon in the ASU oxygen stream is typically propane (C_3H_6). Therefore, the detection limit and interference resistance were paramount to assessing the use of FTIR in this process.

Before running the tests, the FTIR was purged overnight with electronic grade purity nitrogen in both the gas cell area as well as the optics area. The single beam was monitored to demonstrate that no residual gases were in either path. This ensures that an absolutely zero baseline with no minor artifacts will be present such that the remainder will be the residual noise of the baseline (shown in Figure 22).

Three separate gas mixtures (in bulk N_2) were supplied into a gas dilution/mixing system which uses N_2 as the diluting gas. In addition, two single binary gas mixes were used for calibration transfer standard (CTS) (CH_4:N_2) and detection limit (DL) checks (C_3H_8:N_2).

The first check of the FTIR was the **calibration transfer standard** check which is normally performed on any FTIR before a series of runs. This check determines whether the FTIR is performing within specifications. The observed methane concentration of 885.1 ± 0.6 ppm deviates 1.5% from the certified value of 899 ppm, which was well within the accepted variance of 5% for a normal CTS check.

The next checks were for the **calibration validations** using set flows of the four-channel gas mixer. Typical results for each tested gas were as follows (Table 2; * possible slight leak affecting CO2 measurement):

Gas	Average Deviation (%)
C2H6 (ethane)	3.8±0.4 %
CH4 (methane)	0.91±0.44%
C2H4 (ethylene)	4.01±0.27 %
C2H2 (acetylene)	0.36±0.12 %
C3H6 (propylene)	3.67±0.39 %
CO2 (carbon dioxide)*	3.9±1.0%
N2O (nitrous oxide)	1.5±1.1 %

Table 2. Calibration validation results

Following the calibration validations were the **limit of detection** tests (Table 3) for all gases except for propane. The propane test was conducted in a different manner since this gas measurement determines whether the ASU process shuts down. Therefore, a more concise determination of measurement accuracy and bias near its limit of detection was conducted in a following experiment.

Gas	Avg. LOD (3σ) ppm
C2H6 (ethane)	0.11
CH4 (methane)	0.05
C2H4 (ethylene)	0.03
C2H2 (acetylene)	0.03
C3H6 (propylene)	0.08
CO2 (carbon dioxide)	0.01
N2O (nitrous oxide)	0.015

Table 3. Limit of Detection Test results

During the **interference testing or effectiveness (randomized interference) testing,** no major interference bias of propane from most of the tested gases was noted. A representative sample spectrum showing all measured gas components is attached at the end of the discussion to demonstrate the relative overlap of the spectral response for all the components (Figure 23); each component is quantified correctly using classical least squares analysis (CLS) even though their regions have many coincidences. The only truly consistent measurement interference observed was a slight negative bias in the propane measurement (trending to -0.075 ppm) when exposed to high (133 ppm) concentrations of methane. This bias is shown graphically in the following plot (Figure 19). Slight quantification region adjustment will likely improve this. However, being an extreme case of hydrocarbon impurity a level like this would most likely cause ASU process alarming in any case. At reduced methane concentrations, there was little to no observed bias in propane level.

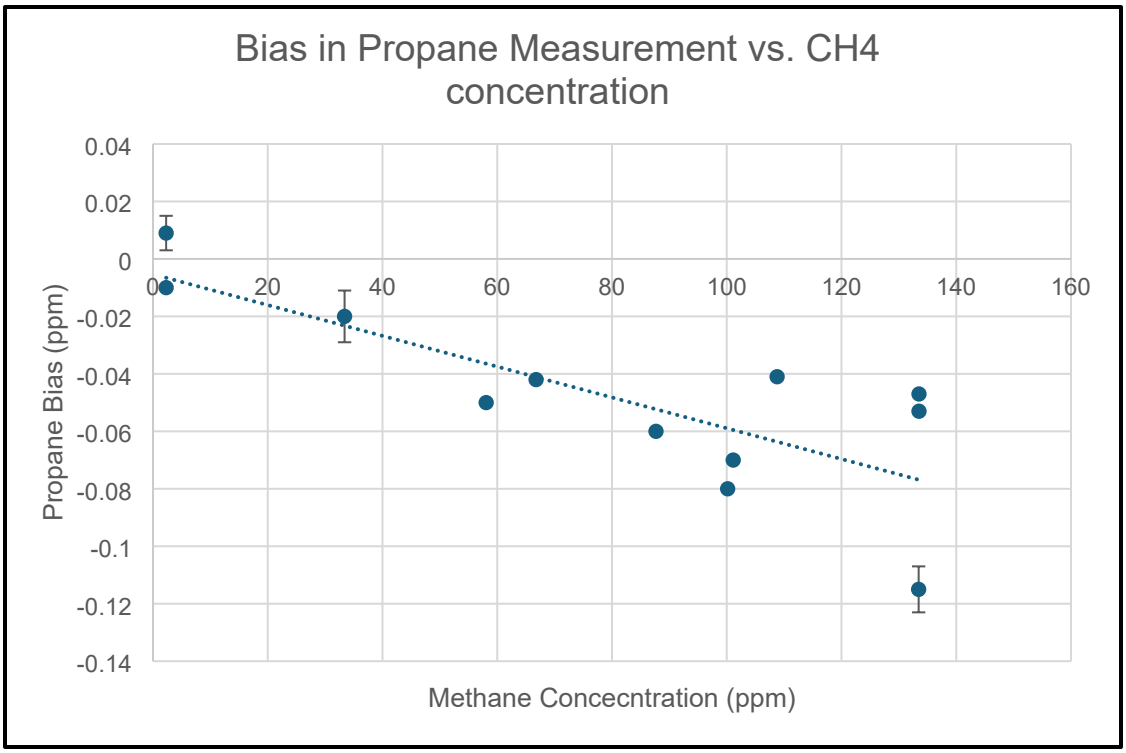


Figure 19. Propane measurement bias vs. methane concentration

Finally, a strict **propane detection limit test** was performed using the binary propane/nitrogen cylinder mix. Both the response linearity and the measurement deviation from predicted are shown in the plots below. A consistent 18 to 27 ppb detection limit was observed throughout this testing; this would be in alignment with the accepted detection limit of 30 ppb noted in previous testing on liquid nitrogen cooled MCT FTIR detection systems.

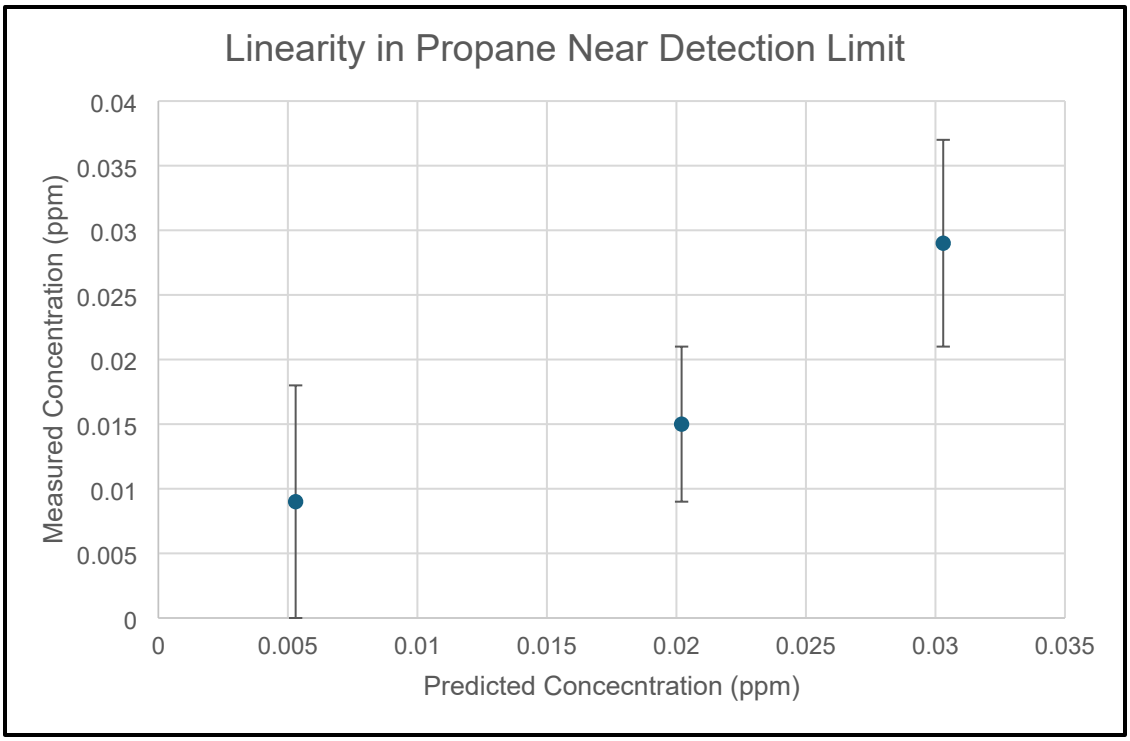


Figure 20. Propane linearity response test

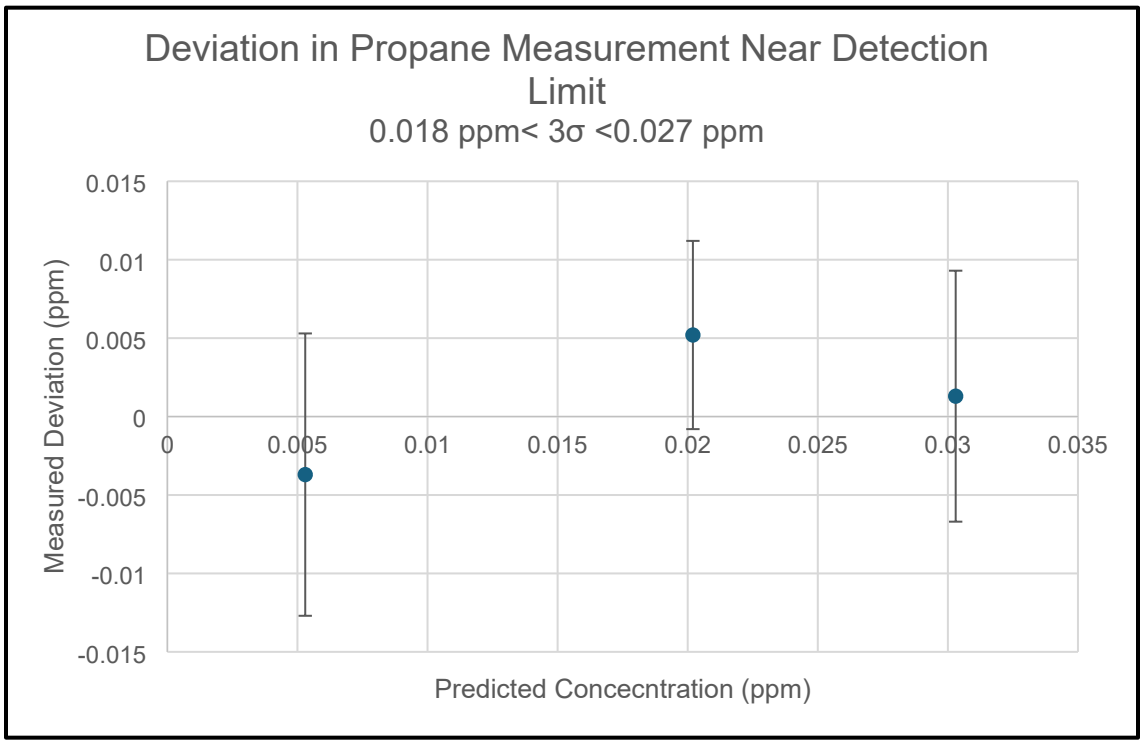


Figure 21. Deviation in propane measurement near detection limit

CONCLUSIONS

1) The DTGS FTIR system performed as expected with no significant deviations in observing individual hydrocarbon concentrations in widely varying mixes.

2) There is a slight negative bias (-0.075 ppm) in the propane measurement when high methane is also present, well beyond any extreme alarm level for an ASU process. Lower levels of methane had little to no effect on the propane measurement.

3) The calculated detection limit for propane was 0.03 ppm, which is equal to that observed with a liquid nitrogen cooled MCT FTIR. The lowest RMS residual noise for 1 minute integration time is on the order of 0.0001 AU (Figure 22).

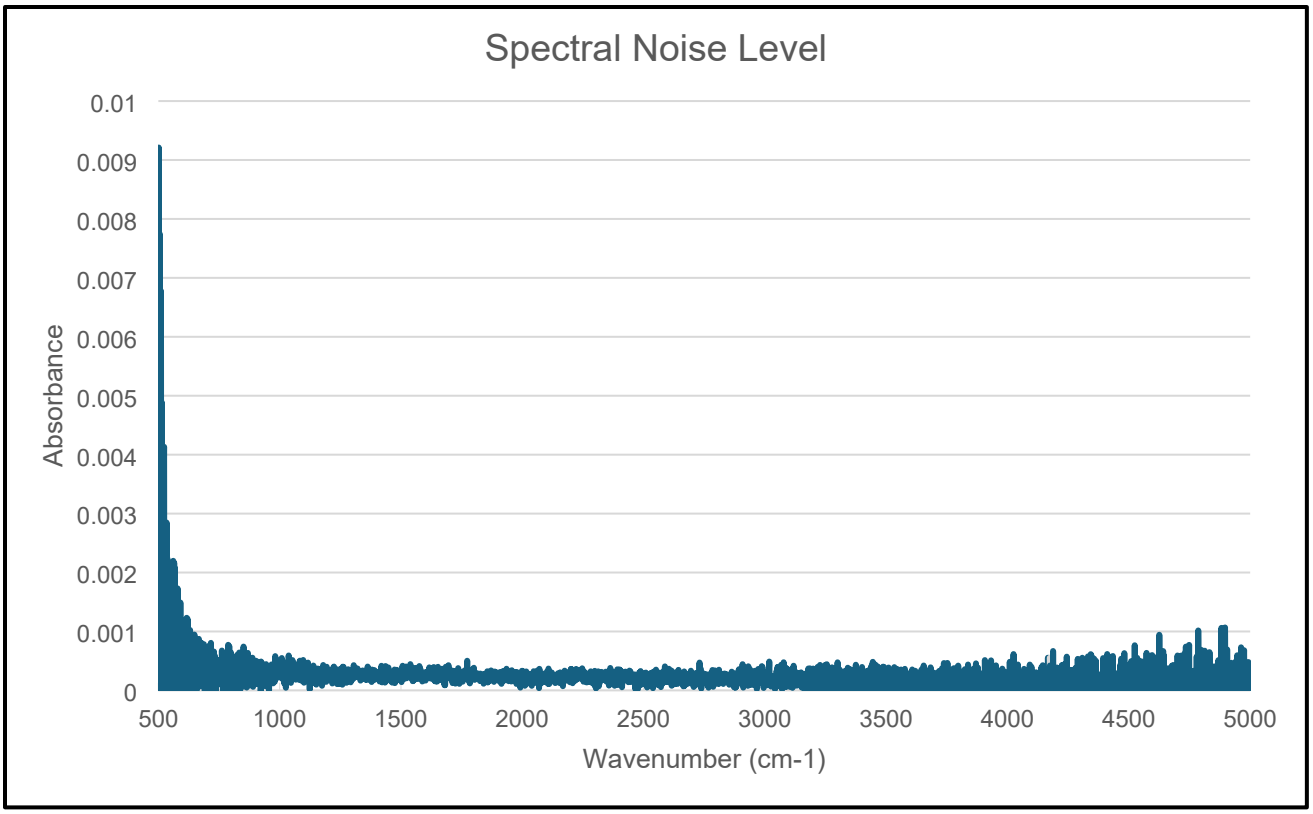


Figure 22. Noise level for 1 minute measure on DTGS FTIR

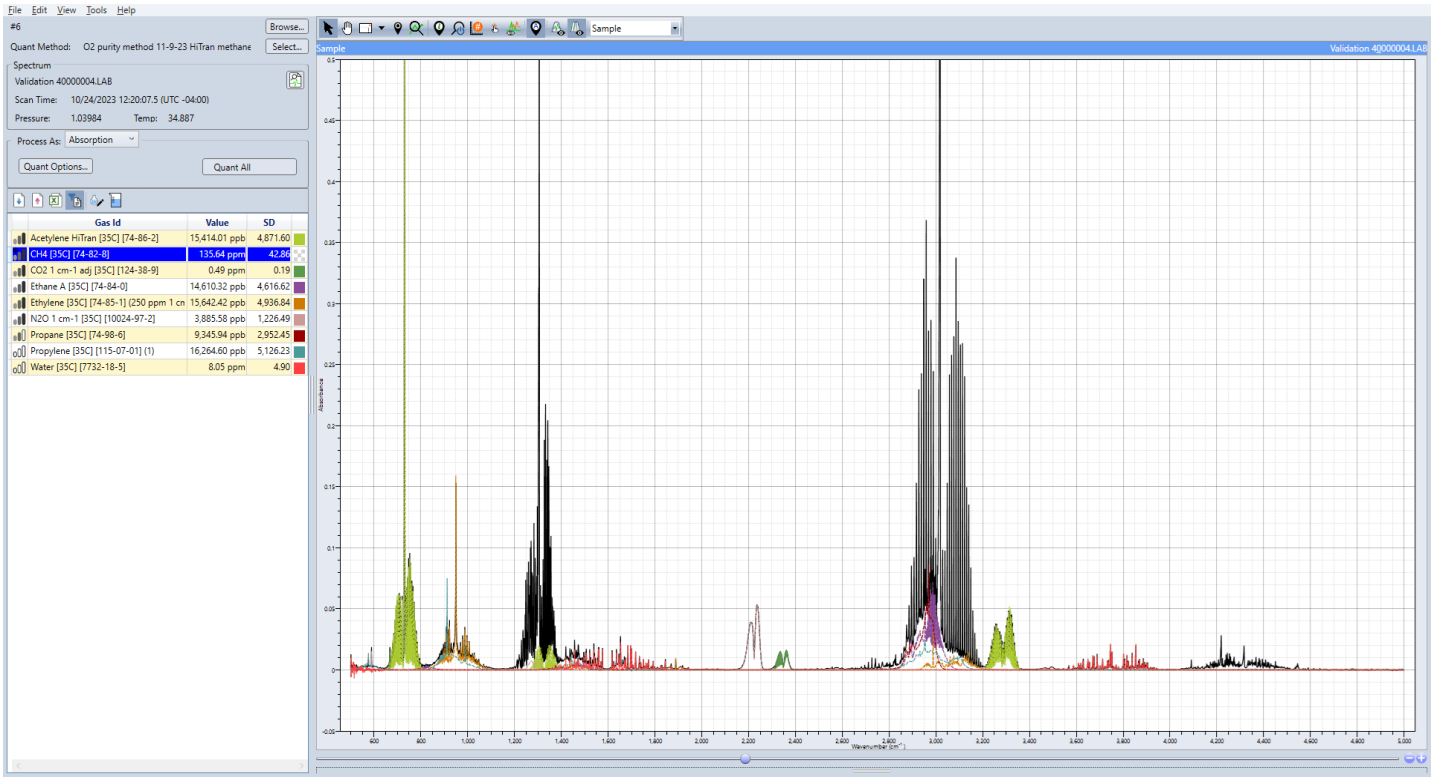


Figure 23. Representative spectra for all gases used in this test